Fractional Brownian motion and motion governed by the fractional Langevin equation in confined geometries

Jae-Hyung Jeon* and Ralf Metzler†

Department of Physics, Technical University of Munich, James-Franck Straße, 85747 Garching, Germany

(Received 30 August 2009; revised manuscript received 21 October 2009; published 1 February 2010)

Motivated by subdiffusive motion of biomolecules observed in living cells, we study the stochastic properties of a non-Brownian particle whose motion is governed by either fractional Brownian motion or the fractional Langevin equation and restricted to a finite domain. We investigate by analytic calculations and simulations how time-averaged observables (e.g., the time-averaged mean-squared displacement and displacement correlation) are affected by spatial confinement and dimensionality. In particular, we study the degree of weak ergodicity breaking and scatter between different single trajectories for this confined motion in the subdiffusive domain. The general trend is that deviations from ergodicity are decreased with decreasing size of the movement volume and with increasing dimensionality. We define the displacement correlation function and find that this quantity shows distinct features for fractional Brownian motion, fractional Langevin equation, and continuous time subdiffusion, such that it appears an efficient measure to distinguish these different processes based on single-particle trajectory data.

DOI: 10.1103/PhysRevE.81.021103 PACS number(s): 05.40.−a, 87.15.Vv, 02.50.−r, 87.10.Mn

I. INTRODUCTION

Anomalous diffusion denominates deviations from the regular linear growth of the mean-squared displacement $\langle \mathbf{r}^2(t)\rangle \simeq K_1 t$ as a function of time t, where the proportionality factor K_1 is the diffusion constant of dimension cm^2/s. Often, these deviations are of power-law form and in this case, the mean-squared displacement in d dimensions

$$\langle \mathbf{r}^2(t)\rangle = \frac{2dK_\alpha}{\Gamma(1+\alpha)} t^\alpha \tag{1.1}$$

describes subdiffusion when the anomalous diffusion exponent is in the range $0<\alpha<1$ and superdiffusion for $\alpha>1$ [1]. The generalized diffusion constant K_α has dimension $\mathrm{cm}^2/\mathrm{s}^\alpha$. We here concentrate on subdiffusion phenomena. Power-law mean-squared displacements of the form (1.1) with $0<\alpha<1$ have been observed in a multitude of systems such as amorphous semiconductors [2], subsurface tracer dispersion [3], or in financial market dynamics [4]. Subdiffusion is quite abundant in small systems. These include the motion of small probe beads in actin networks [5], local dynamics in polymer melts [6], or the motion of particles in colloidal glasses [7]. *In vivo*, crowding-induced subdiffusion has been reported for RNA motion in *E. coli* cells [8], the diffusion of lipid granules embedded in the cytoplasm [9,10], the propagation of virus shells in cells [11], the motion of telomeres in mammalian cells [12], as well as the diffusion of membrane proteins and of dextrane probes in HeLa cells [13].

While the mean-squared displacement Eq. (1.1) is commonly used to classify a process as subdiffusive, it does not provide any information on the physical mechanism underlying this subdiffusion. In fact, there are several pathways along which this subdiffusion may emerge. The most common are:

(i) The continuous time random walk (CTRW) [2] in which the step length has a finite variance $\langle \delta\mathbf{r}^2\rangle$ of jump lengths, but the waiting time τ elapsing between successive jumps is distributed as a power law $\psi(\tau)\simeq \tau_0^\alpha/\tau^{1+\alpha}$, with $0<\alpha<1$. The diverging characteristic waiting time gives rise to subdiffusion of the form (1.1) [2]. The subdiffusive CTRW in the diffusion limit is equivalent to the fractional Fokker-Planck equation that directly shows the long-ranged memory intrinsic to the process [1]. Waiting times of the form $\psi(\tau)$ were, for instance, observed in the motion of tracer beads in an actin network [5]. We note that recently, subdiffusion was also demonstrated in a coupled CTRW [14].

(ii) A random walk on a fractal support meets bottlenecks and dead ends on all scales and is subdiffusive. The resulting subdiffusion is also of the form (1.1) and the anomalous diffusion exponent is related to the fractal and spectral dimensions, d_f and d_s, characteristic of the fractal, through $\alpha = d_s/d_f$ [15]. A typical example is the subdiffusion on a percolation cluster near criticality that was actually verified experimentally [16].

(iii) Fractional Brownian motion (FBM) and the fractional Langevin equation (FLE) that will be in the focus of this work and will be defined in Sec. II. The understanding of these types of stochastic motions is up to date somewhat fragmentary. Thus, the first passage behavior of FBM is known analytically only in one dimension on a semi-infinite domain [17], the escape from potential wells in the framework of FLE has been studied analytically [18,19] and numerically [20,21], and *a priori* unexpected critical exponents have been identified for the FLE [22]. Here we address a fundamental question related to FBM and FLE. Namely, what is their behavior under confinement? Two main aspects of this question will be addressed. One is the study of the relaxation toward stationarity in a finite box by means of the ensemble-averaged mean-squared displacement. We also in-

*jae-hyung.jeon@ph.tum.de
†metz@ph.tum.de

 ©2010 The American Physical Society

vestigate a new quantity used to characterize the motion, the displacement correlation function. For these aspects, we also study the dependence on the dimensionality of the motion.

The second aspect concerns how FBM and FLE motions under confinement behave with respect to ergodicity. Experimentally, the recording of single-particle trajectories has become a standard tool, producing time series of data that are then analyzed by time rather than ensemble averages. For subdiffusion processes, both are not necessarily identical. In fact, for CTRW subdiffusion with an ensemble-averaged mean-squared displacement of the form (1.1), the time-averaged mean-squared displacement

$$\overline{\delta^2(\Delta,T)} = \frac{1}{T-\Delta}\int_0^{T-\Delta}[x(t+\Delta)-x(t)]^2 dt \qquad (1.2)$$

on average scales like $\langle\overline{\delta^2(\Delta,T)}\rangle \simeq \Delta/T^{1-\alpha}$ [23,24]. That is, the anomalous diffusion is manifested only in the dependence on the overall measurement time T and not in the lag time Δ that defines a window swept along the time series. Thus, time and ensemble averages are indeed different. In contrast, for normal Brownian diffusion, $\langle\overline{\delta^2(\Delta,T)}\rangle \simeq \Delta$ is independent of T and time and ensemble averages become identical, i.e., the system is ergodic. Different from CTRW subdiffusion, systems governed by FBM or FLE are ergodic. The ergodicity-breaking parameter measured from time-averaged mean-squared displacements converges algebraically to zero (ergodic behavior) as the measurement time increases, the convergence speed depending on the Hurst exponent $H=\alpha/2$ [25]. For the FLE case, however, it was also shown that the ergodicity measured from the velocity variance can be broken for a class of colored noises [26].

One of the open questions in the context of ergodicity breaking for FBM and FLE in the above sense is the influence of boundary conditions on the time averages. It was shown for CTRW subdiffusion that confinement changes the short-time scaling $\langle\overline{\delta^2(\Delta,T)}\rangle \simeq \Delta/T^{1-\alpha}$ to the long-time behavior $\langle\overline{\delta^2(\Delta,T)}\rangle \simeq (\Delta/T)^{1-\alpha}$ [27,28]. Although we expect that FBM and FLE processes become stationary under confinement and, for instance, attain the same long-time mean-squared displacement dictated by the size of the confinement volume, we investigate how fast this relaxation actually is and how it depends on the volume and the dimensionality. To this end, we study the ergodicity-breaking parameter for the system. We find that for both FBM and FLE confinements actually decrease the value of the ergodicity-breaking parameter with respect to unbounded motion, i.e., the process becomes more ergodic. Ergodicity is also enhanced with increasing dimensionality. We also discuss how FBM and FLE motions can be distinguished from time series from single-particle trajectories.

The paper is organized as follows. In Sec. II, we present FBM and FLE motions and review briefly their basic statistical properties. In Sec. III, we describe the numerical scheme for simulating FBM and FLE in confined space. Simulation results are presented in Secs. IV and V, where we discuss the effects of confinement and dimensionality on time-averaged mean-squared displacement trajectory, ergodicity, and displacement correlation. We draw our conclusions in Sec. VI.

II. THEORETICAL MODEL

We here define FBM and FLE. These two stochastic models share many common features, however, their physical nature is different. In the following, we will see, in particular, how the two can be distinguished on the basis of experimental or simulations data.

A. Fractional Brownian motion

FBM was originally introduced by Kolmogorov in 1940 [29] and further studied by Yaglom [30]. In a different context, it was introduced by Mandelbrot in 1965 [31] and fully described by Mandelbrot and van Ness in 1968 in terms of a stochastic integral representation [32]. In the latter reference, the authors wrote that "we believe FBMs do provide useful models for a host of natural time series." This study was motivated by Hurst's analysis of annual river discharges [33], the observation that in economic time series cycles of all orders of magnitude occur [34], and that many experimental studies exhibit the now famed $1/f$ noise. FBM by now is widely used across fields. Among many others, FBM has been identified as the underlying stochastic process of the subdiffusion of large molecules in biological cells [13,35,36]. We note that FBM is neither a semimartingale nor a Markov process, which makes it quite intricate to study with the tools of stochastic calculus [37,38].

FBM, $x^H(t)$, is a Gaussian process with stationary increments which satisfies the following statistical properties: the process is symmetric,

$$\langle x^H(t)\rangle = 0, \qquad (2.1)$$

with $x^H(0)=0$, and the second moment scales like Eq. (1.1),

$$\langle x^H(t)^2\rangle = 2K_H t^{2H}. \qquad (2.2)$$

For easier comparison to other literature, we introduced the Hurst exponent H that is related to the anomalous diffusion exponent via $H=\alpha/2$. The Hurst exponent may vary in the range $0<H<1$, such that FBM describes both subdiffusion $(0<H<1/2)$ and superdiffusion $(1/2<H<1)$. The limits $H=1/2$ and $H=1$ correspond to Brownian and ballistic motion, respectively. Finally, the two-point correlation behaves as

$$\langle x^H(t_1)x^H(t_2)\rangle = K_H(t_1^{2H}+t_2^{2H}-|t_1-t_2|^{2H}). \qquad (2.3)$$

Here, $\langle\cdot\rangle$ represents the ensemble average. It is convenient to introduce fractional Gaussian noise (FGN), $\xi^H(t)$ from which the FBM is generated by

$$x^H(t) = \int_0^t dt'\,\xi^H(t'). \qquad (2.4)$$

FGN has the properties of zero mean

$$\langle\xi^H(t)\rangle = 0 \qquad (2.5)$$

and autocorrelation [39,40]

$$\langle \xi^H(t_1)\xi^H(t_2)\rangle = 2K_H H(2H-1)|t_1-t_2|^{2H-2} + 4K_H H|t_1-t_2|^{2H-1}\delta(t_1-t_2), \quad (2.6)$$

as can be seen by differentiation of Eq. (2.3) with respect to t_1 and t_2. Here we see that K_H plays the role of a noise strength. For subdiffusion $(0<H<1/2)$, the autocorrelation is negative for $t_1 \neq t_2$, i.e., the process is anticorrelated or antipersistent [41]. In contrast, for $1/2<H<1$, the noise is positively correlated (persistent) and the motion becomes superdiffusive. For normal diffusion $(H=1/2)$, the noise is uncorrelated, i.e., $\langle \xi^H(t_1)\xi^H(t_2)\rangle = 2K_H\delta(t_1-t_2)$. For further details, compare the discussions in Refs. [32,42].

We define d-dimensional FBM as a superposition of independent FBMs for each Cartesian coordinate such that

$$\mathbf{x}^H(t) = \sum_{i=1}^{d} \int_0^t dt' \xi_i^H(t')\hat{x}_i, \quad (2.7)$$

where $\hat{x}_i$ is the Cartesian coordinate of the ith component and ξ_i^H is FGN which satisfies

$$\langle \xi_i^H(t)\rangle = 0 \quad (2.8)$$

and

$$\langle \xi_i^H(t_1)\xi_j^H(t_2)\rangle = 2K_H H(2H-1)|t_1-t_2|^{2H-2}\delta_{ij} + 4K_H H|t_1-t_2|^{2H-1}\delta(t_1-t_2)\delta_{ij}. \quad (2.9)$$

From this definition, d-dimensional FBM $\mathbf{x}^H(t)$ has the properties of zero mean

$$\langle \mathbf{x}^H(t)\rangle = 0, \quad (2.10)$$

variance

$$\langle \mathbf{x}^H(t)^2\rangle = 2dK_H t^{2H}, \quad (2.11)$$

and autocorrelation

$$\langle \mathbf{x}^H(t_1)\cdot\mathbf{x}^H(t_2)\rangle = dK_H(t_1^{2H}+t_2^{2H}-|t_1-t_2|^{2H}). \quad (2.12)$$

Note that $|\mathbf{x}^H(t)|$ cannot satisfy these properties, thus it is not an FBM.

A few remarks on this multidimensional extension of FBM are in order. We note that, albeit intuitive due to the Gaussian nature of FBM, this multidimensional extension is not necessarily unique. In mathematical literature, higher-dimensional FBM in the above sense was defined in Refs. [43,44]. In physics literature, an analogous extension to higher dimensions was used in Ref. [13] based on the Weierstrass-Mandelbrot method (Note: HeLa cells belong to an immortal cell line derived from cancer cells originally taken from Henrietta Lacks in 1951, see Ref. [13]). To verify that this d-dimensional extension is meaningful, we checked from our simulations of d-dimensional FBM that the fractal dimension of FBM, $d_f=1/H$ for $H>1/d$ [45], is preserved in higher dimensions. Moreover, we used an alternative method to create FBM in d dimensions, namely, to use one-dimensional (1D) FBM to choose the length of a radius and then choose the space angle randomly. The results were equivalent to the above definition to use independent FBMs for every Cartesian coordinate. We are therefore confident that our definition of FBM in d dimensions is a proper extension of regular 1D FBM.

B. Fractional Langevin equation motion

An alternative approach to Brownian motion is based on the Langevin equation [46–48]

$$m\frac{d^2y(t)}{dt^2} = -\bar{\gamma}\frac{dy(t)}{dt} + \xi(t), \quad (2.13)$$

where $\xi(t)$ corresponds to white Gaussian noise. When the random noise $\xi(t)$ is nonwhite, the resulting motion is described by the generalized Langevin equation (GLE)

$$m\frac{d^2y(t)}{dt^2} = -\bar{\gamma}\int_0^t \mathcal{K}(t-t')\frac{dy}{dt'}dt' + \xi(t), \quad (2.14)$$

where m is the test particle mass and $\mathcal{K}$ is the memory kernel [49–51] which satisfies the fluctuation-dissipation theorem $\langle \xi(t)\xi(t')\rangle = k_B T\bar{\gamma}\mathcal{K}(t-t')$. When ξ is the FGN introduced above, $\mathcal{K}$ decays algebraically and Eq. (2.14) becomes the FLE

$$m\frac{d^2y(t)}{dt^2} = -\bar{\gamma}\int_0^t (t-t')^{2\bar{H}-2}\frac{dy}{dt'}dt' + \eta\xi^{\bar{H}}(t) = -\bar{\gamma}\Gamma(2\bar{H}-1)\frac{d^{2-2\bar{H}}}{dt^{2-2\bar{H}}}y(t) + \eta\xi^{\bar{H}}(t). \quad (2.15)$$

Here, $\bar{\gamma}$ is a generalized friction coefficient. We also define the coupling constant

$$\eta = \sqrt{\frac{k_B T\bar{\gamma}}{2K_H\bar{H}(2\bar{H}-1)}} \quad (2.16)$$

imposed by the fluctuation dissipation theorem and the Caputo fractional derivative [52]

$$\frac{d^{2-2\bar{H}}}{dt^{2-2\bar{H}}}y(t) = \frac{1}{\Gamma(2\bar{H}-1)}\int_0^t dt'(t-t')^{2\bar{H}-2}\frac{dy}{dt'}. \quad (2.17)$$

Note that in Eq. (2.15), the memory integral diverges for $\bar{H}$ smaller than 1/2, such that the Hurst exponent in the FLE is restricted to the range $1/2<\bar{H}<1$.

It can be shown that the relaxation dynamics governed by the FLE (2.15) follows the form

$$\langle y(t)\rangle = v_0 t E_{2\bar{H},2}(-\gamma t^{2\bar{H}}) \quad (2.18)$$

for the first moment, where v_0 is the initial particle velocity. The rescaled friction coefficient is $\gamma=\bar{\gamma}\Gamma(2\bar{H}-1)/m$. The coordinate variance behaves as

$$\langle y^2(t)\rangle = 2\frac{k_B T}{m}t^2 E_{2\bar{H},3}(-\gamma t^{2\bar{H}}), \quad (2.19)$$

where $\langle v_0^2\rangle = k_B T/m$ is assumed, and we employed the generalized Mittag-Leffler function [53]

$$E_{\alpha,\beta}(z) = \sum_{n=0}^{\infty} \frac{z^n}{\Gamma(\alpha n + \beta)}, \tag{2.20}$$

whose asymptotic behavior for large z is

$$E_{\alpha,\beta}(z) = -\sum_{n=1}^{\infty} \frac{z^{-n}}{\Gamma(\beta - \alpha n)}. \tag{2.21}$$

Thus, the mean-squared displacement shows a turnover from short-time ballistic motion to long-time anomalous diffusion of the form [54,55]

$$\langle y^2(t)\rangle \sim \begin{cases} t^2, & t \to 0 \\ t^{2-2\bar{H}}, & t \to \infty. \end{cases} \tag{2.22}$$

Therefore, for persistent noise with $1/2 < \bar{H} < 1$, the resulting motion is in fact subdiffusive, i.e., the persistence of the noise has the opposite effect than in FBM.

In analogy to our discussion of FBM in a d-dimensional embedding, the FLE is generalized to

$$m\frac{d^2\mathbf{y}(t)}{dt^2} = -\bar{\gamma}\int_0^t \vec{\vec{\mathcal{K}}} \cdot \frac{d\mathbf{y}}{dt'}dt' + \boldsymbol{\xi}(t), \tag{2.23}$$

where $\mathbf{y}(t) = \Sigma_i y_i(t)\hat{x}_i$, $\boldsymbol{\xi}(t) = \Sigma_i \xi_i^H(t)\hat{x}_i$, and $\vec{\vec{\mathcal{K}}}$ is the memory tensor which is in diagonal form [i.e., $\mathcal{K}_{ij} = \mathcal{K}(t-t')\delta_{ij}$] in the absence of motional coupling between different coordinates.

III. SIMULATIONS SCHEME

We here briefly review the simulations scheme used to produce time series for FBM and FLE motions.

A. Fractional Brownian motion

d-dimensional FBM is simulated via Eq. (2.7) by numerical integration of $\xi_i^H(t)$. The underlying FGN was generated by the Hosking method which is known to be an exact but time-consuming algorithm [56]. We checked that in the one-dimensional case, the generated FBM in free space successfully reproduces the theoretically expected behavior, the mean-squared displacement (1.1), the fractal dimension $d_f = 2 - \alpha/2$ of the resulting trajectory, and the first passage time distribution. To simulate the confined motion, reflecting walls were considered at locations $\pm L$ for each coordinate. For instance in the 1D case, if $|x^H(t)| > L$ at some time t, the particle bounces back to the position $x^H(t) - 2|x^H(t) - \mathrm{sgn}(x^H)L|$. Similar reflecting conditions were taken into account in the multidimensional case.

B. Fractional Langevin equation motion

In simulating FLE motion, we follow the numerical method presented by Deng and Barkai [25]. First, integrating Eq. (2.15) from 0 to t, we obtain the Volterra integral equation for velocity field $v(t) = dy(t)/dt$,

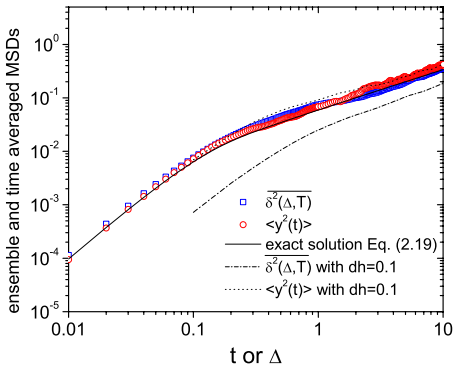

FIG. 1. (Color online) The mean-squared displacements (MSDs) for FLE motion in free space. The ensemble-averaged and time-averaged MSDs, $\langle y^2(t)\rangle$ and $\langle\overline{\delta^2(\Delta,T)}\rangle$, obtained from simulation are compared to the exact solution $2t^2E_{5/4,3}[-10\Gamma(5/4-1)t^{5/4}]$ given by Eq. (2.19). The numerical values were obtained from 200 simulated trajectories. In the simulation, we chose the Hurst exponent $\bar{H} = 5/8$, time increment $dh = 0.01$, particle mass $m = 1$, initial velocity $v_0 = 1$, initial position $y_0 = 0$, friction coefficient $\bar{\gamma} = 10$, and $k_BT = 1$.

$$v(t) = -\frac{\bar{\gamma}}{(2\bar{H}-1)m}\int_0^t (t-t')^{2\bar{H}-1}v(t')dt' + v_0 + \frac{\eta}{m}x^{\bar{H}}(t), \tag{3.1}$$

where $v(t=0) = v_0$. This stochastic integral equation can be evaluated by the predictor-corrector algorithm presented in Ref. [57] with the FBM $x^{\bar{H}}(t)$ independently obtained by the Hosking method. We calculated $y(t) = y_0 + \int_0^t v(t')dt'$ by the trapezoidal algorithm. For discrete time steps, the equation of motion is given by

$$y_{n+1} = y_0 + \frac{dh}{2}(v_0 + v_{n+1}) + dh\sum_{i=1}^{n} v_i,$$

$$= \frac{dh}{2}(v_n + v_{n+1}) + y_n, \tag{3.2}$$

where dh is the time increment. When evaluating Eq. (3.2), a reflecting boundary condition was considered in the sense that $y_n \to y_n - 2|y_n - \mathrm{sgn}(y_n)L|$ if $|y_n| > L$.

To show the reliability of our simulation, we compare the simulation result to the well-known solution for free space motion. In Fig. 1 we simulate the subdiffusion case with the parameters values $\bar{H} = 5/8$, $m = 1$, $v_0 = 1$, $y_0 = 0$, $\bar{\gamma} = 10$, $k_BT = 1$, and $dh = 0.01$. From 200 simulated trajectories, we obtain the ensemble-averaged and time-averaged mean-squared displacements, $\langle y^2(t)\rangle$ and $\langle\overline{\delta^2(\Delta,T)}\rangle$, and compare them to the exact solution Eq. (2.19). Note that $\langle y^2(t)\rangle$ should be identical to $\langle\overline{\delta^2(\Delta,T)}\rangle$, Eq. (5.2), with t regarded as the lag time Δ due to the ergodicity of the FLE motion in free space [25]. The deviation from the exact solution is markedly reduced with decreasing time increment dh. With our chosen value $dh = 0.01$, the mean-squared displacements obtained from simulation appear to be in good agreement with the theory (Fig. 1).

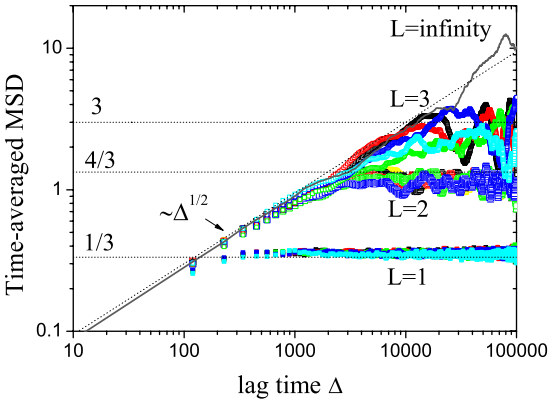

FIG. 2. (Color online) Time-averaged MSD vs the lag time Δ for given values of L. The drawn line has slope 1/2, corresponding to the expected short lag time behavior for the used value $H=1/4$ of the Hurst exponent. For $L=1$, 2, and 3, five different trajectories each are drawn to be able to see whether the trajectories scatter. The simulation time is $T=2^{17}\approx 1.3\times 10^5$.

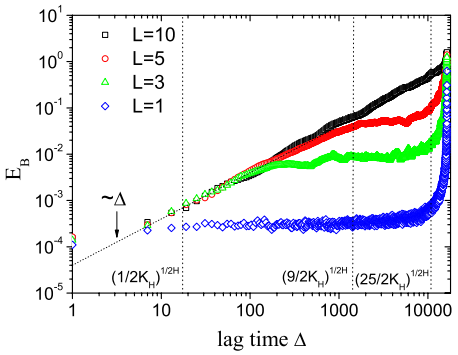

FIG. 3. (Color online) Ergodicity-breaking parameter E_B vs lag time Δ for $L=1$, 3, 5, and 10 (from bottom to top) with Hurst exponent $H=1/4$. The overall measurement time is $T=2^{14}\approx 1.6\times 10^4$. Dotted line with slope 1 represents the theoretical expectation $E_B\simeq\Delta$ in free space. For each L, the curve was obtained from 200 single trajectories. Vertical lines show the crossover lag time $\Delta_{cr}=(L^2/2K_H)^{1/2H}$ for $L=1$, 3, and 5.

IV. FRACTIONAL BROWNIAN MOTION IN CONFINED SPACE

We now turn to the investigation of the behavior of FBM under confinement, analyzing the mean-squared displacement and potential ergodicity breaking. We then define the displacement correlation function and finally study the influence of dimensionality.

A. Mean-squared displacement

For FBM in free space $\langle x^H(t)^2\rangle$ can be estimated by the time-averaged mean-squared displacement Eq. (1.2) via the exact relation [25]

$$\langle\overline{\delta^2(\Delta,T)}\rangle = 2K_H\Delta^{2H}. \tag{4.1}$$

Here, $\langle\cdot\rangle$ denotes the ensemble average. In contrast to CTRW subdiffusion, in FBM, this quantity is ergodic. However, as mentioned above, the approach to ergodicity is algebraically slow and we want to explore here whether boundary conditions have an impact on the ergodic behavior. Let us now analyze the behavior in a box of size $2L$.

In Fig. 2, we show typical curves for the time-averaged mean-squared displacement for Hurst exponent $H=1/4$ and three different interval lengths L. Regardless of the size of L, the confined environment does not affect the power law with exponent $2H$ for short lag times. Moreover, at long lag times, we observe saturation of the curves to a value that depends on L. This behavior is distinct from that of the CTRW case where $\langle\overline{\delta^2(\Delta,T)}\rangle$ shows a power law with slope $1-\alpha$ [27,28].

One can estimate the saturated value as a function of L. For long Δ and measurement time T, the probability $p(x)$ to find the particle located at x is independent of x due to the equilibration between the reflecting walls and thus $\int_{-L}^{L}x^2p(x)dx=L^2/3$. The dotted lines in Fig. 2 represent these values.

We observe that the scatter between different single trajectories becomes more pronounced when the interval length is increased. In fact, the scatter is negligible for $L=1$ while it is quite appreciable for $L=3$, even though the slope of all curves at finite L converges to a horizontal slope, with an amplitude close to the predicted value $L^2/3$. We also note that the scatter depends on the total measurement time T. For given L, it tends to be reduced as we increase T. This effect will be discussed quantitatively in detail using the ergodicity-breaking parameter.

B. Ergodicity-breaking parameter

In contrast to CTRW subdiffusion, FBM in free space is known to be ergodic [25]. The time-averaged mean-squared displacement traces displayed in Fig. 2 exhibit no extreme scatter as known from the CTRW case. This implies that ergodicity is indeed preserved for confined FBM. We quantify this statement more precisely in terms of the ergodicity-breaking parameter [23]

$$E_B(\Delta,T)=\frac{\langle[\overline{\delta^2(\Delta,T)}]^2\rangle-\langle\overline{\delta^2(\Delta,T)}\rangle^2}{\langle\overline{\delta^2(\Delta,T)}\rangle^2}, \tag{4.2}$$

where $\lim_{T\to\infty}E_B(T)=0$ is expected for ergodic systems. For the case of free FBM, Deng and Barkai analytically derived that E_B decays to zero as

$$E_B(\Delta,T)\sim\begin{cases}\dfrac{\Delta}{T} & \text{for } 0<H<\frac{3}{4}\\ \dfrac{\Delta}{T}\log T & \text{for } H=\frac{3}{4}\\ \left(\dfrac{\Delta}{T}\right)^{4-4H} & \text{for } \frac{3}{4}<H<1\end{cases} \tag{4.3}$$

for long measurement time T [25].

We numerically investigate the boundary effects on the ergodicity-breaking parameter. First, in Fig. 3, we evaluate E_B as function of the lag time Δ from 200 FBM simulations for each given L. The dotted line represents the expected free-space behavior $E_B\sim\Delta$, which is nicely fulfilled by the data at shorter times and sufficiently large L. At longer times

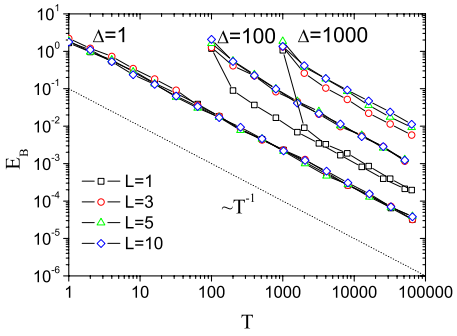

FIG. 4. (Color online) Ergodicity-breaking parameter E_B vs overall measurement time T at given lag times $\Delta=1$, 100, and 1000. Dotted line depicts a power law with slope −1, representing the analytic behavior $E_B \simeq T^{-1}$ in free space. For each Δ, the E_B curves are drawn for different interval lengths $L=1$, 3, 5, and 10. Each curve was obtained from 200 single trajectories and the Hurst exponent was $H=1/4$.

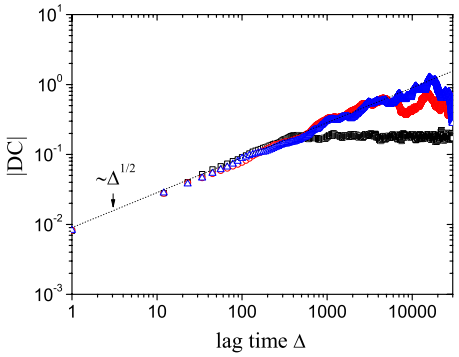

FIG. 5. (Color online) Absolute value of the displacement correlation (DC) vs lag time Δ for $L=1$, 2, and 3 (from bottom to top) with a slope proportional to Δ^{2H} (dotted line). Total measurement time is $T=2^{17}\approx 1.3\times 10^5$ and the Hurst exponent is $H=1/4$. Each curve was obtained via time averaging from a single-particle trajectory.

or small L, the results show that E_B behaves very differently when confinement effects are present. The plateau in E_B is related to the saturation of the curves for the mean-squared displacement, Fig. 2. As the motion is restricted by the walls roughly above a crossover lag time $\Delta_{cr}=(L^2/2K_H)^{1/2H}$, the ergodicity-breaking parameter E_B levels off at $\Delta \gtrsim \Delta_{cr}$. The sharp increase at the end of the curve is due to the singularity when the lag time reaches the size of the overall measurement time T, which would disappear in the infinite measurement time.

In Fig. 4, we show E_B for given Δ as function of the measurement time T for the same choice of interval lengths, $L=1$, 3, 5, and 10. For short lag times Δ, all E_B curves coincide and decay as T^{-1}, in complete analogy to the free-space motion (dotted line). In the case of longer Δ, the general trend is that E_B decays like T^{-1}, unaltered with respect to the free case. However, there is a sudden decrease in E_B for the smallest interval size, for $L=1$. One can understand this behavior by observing the E_B curve for $L=1$ in Fig. 3; as the fluctuations of the mean-squared displacement are strongly suppressed due to the tight confinement in this case, E_B has almost no dependence on Δ for $\Delta_{cr} \lesssim \Delta \lesssim T$ and the saturated value is quite small compared to those for other cases. Therefore, the curves for $L=1$ appear disconnected from the other curves. Corresponding to the approximate independence of the $L=1$ curve for $\Delta \gtrsim 10$ in Fig. 3, we observe in Fig. 4 that at longer times T, the $L=1$ curves approach each other. Only at $T \approx \Delta$ these curves separate, as then $\overline{\delta_i^2(T,T)}=[x_i^H(t+T)-x_i^H(t)]^2$, and E_B is evaluated with the same small number of squared displacement data. Note that the splitting of the E_B curve can be also observed for larger L at Δs larger than Δ_{cr} under longer total measurement time T as other E_B curves also have corresponding constant saturation values for $\Delta \gtrsim \Delta_{cr}[=(L^2/2K_H)^{1/2H}]$ which increases with the size L.

C. Displacement correlation function

As explained for the stochastic properties of FBM in Sec. II, the position autocorrelation $\langle x^H(t_1)x^H(t_2)\rangle$ explicitly depends on t_1 and t_2 as well as their difference, $|t_1-t_2|$. It is therefore not an efficient quantity to estimate directly from experimental or simulations data. However, the correlation function of the displacements

$$\delta x^H(t,\Delta) = x^H(t+\Delta) - x^H(t) \tag{4.4}$$

depends only on the time interval Δ of the displacement

$$\langle \delta x^H(t,\Delta)\, \delta x^H(t-\Delta,\Delta)\rangle = K_H(2^{2H}-2)\Delta^{2H} \tag{4.5}$$

for free FBM. This relation is derived in Appendix A. This quantity is anticorrelated for $0<H<1/2$ (subdiffusive motion), uncorrelated for $H=1/2$ (normal Brownian motion), and positively correlated for $1/2<H<1$ (superdiffusion). As Eq. (4.5) does not depend on the measurement time T, the value of the ensemble averaged value is identical to the corresponding time average.

We present the time-averaged displacement correlation function for confined subdiffusive motion ($H=1/4$) in Fig. 5. Because of the negativity of expression (4.5), the absolute value of the displacement correlation is drawn in the log-log representation. At short lag times, the slope of the correlation functions is proportional to $2H$ as expected from Eq. (4.5). However, at long lag times, we interestingly observe fluctuations of the correlations around a constant value, reflecting the confinement of the motion.

D. Dimensionality

To mimic the anomalous diffusion of particles inside biological cells, we also simulate two- and three-dimensional FBMs based on Eq. (2.7) in the presence of reflecting walls. In free space, the ensemble average of the time-averaged mean-squared displacement is simply given by

$$\langle \overline{\delta^2(\Delta,T)} \rangle = \frac{1}{T-\Delta}\int_0^{T-\Delta} \langle [\mathbf{x}^H(t+\Delta)-\mathbf{x}^H(t)]^2\rangle dt,$$

$$= 2dK_H\Delta^{2H}, \tag{4.6}$$

i.e., it is additive as for the ensemble average. This behavior is indeed observed in Fig. 6 where five different mean-

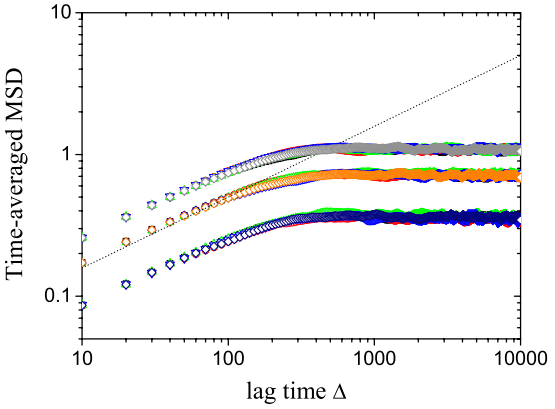

FIG. 6. (Color online) Time-averaged MSD curves vs lag time Δ for $L=1$ in 1D, 2D, and 3D spaces (from bottom to top) with a slope Δ^{2H} (dotted line). For each dimension, five trajectories were drawn with total measurement time $T=2^{17}$ and $H=1/4$.

squared displacement curves are drawn for $L=1$ in 1D, two dimensions (2D), and three dimensions (3D), respectively. Only the height of the curves is affected by the dimensionality. There is no noticeable difference in the scatter of the curves.

We further investigate the effects of dimensionality on the scatter of the mean-squared displacement curves, as possibly the strong scatter observed in experiments [8–10] may also occur for FBM in higher dimensions. To see the effect of dimensionality on the ergodicity behavior, we measure E_B versus lag time for one-, two-, and three-dimensional embedding dimensions for the same values of L and H. Interestingly, the result shows that E_B tends to decrease with increasing dimensionality d, meaning that for FBM, big scatter is not caused by higher dimensions in presence of reflecting walls. In fact, from Eqs. (4.2) and (4.6), we can analytically derive the relation

$$E_B(d) = \frac{E_B(d=1)}{d}, \tag{4.7}$$

which still holds in the case of confined motion (see Appendix B for the derivation). This relation is numerically confirmed in Fig. 7 where three E_B curves collapse upon rescaling by $dE_B(d)$. According to this relation, we expect that ergodic behavior obtained in one-dimensional confined motion (Figs. 3 and 4) will also be present in multiple dimensions with a factor of $1/d$.

V. FRACTIONAL LANGEVIN EQUATION MOTION IN CONFINED SPACE

In this section, we analyze FLE motion under confinement. Due to the different physical basis compared to FBM, in particular, the occurrence of inertia, we observe interesting variations on the properties studied in the previous section.

A. Mean-squared displacement

Using the correlation function [55]

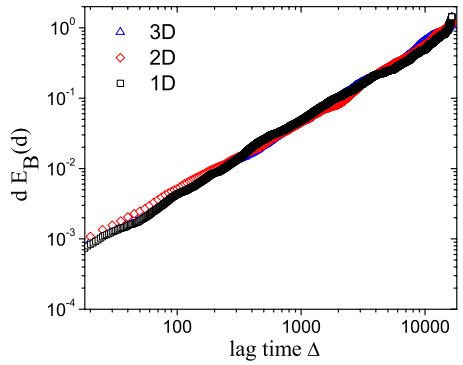

FIG. 7. (Color online) Rescaled ergodicity-breaking parameter vs lag time Δ for interval size $L=5$ for 1D, 2D, and 3D spaces (from top to bottom) with Hurst exponent $H=1/4$ and measurement time $T=2^{14}$. E_B was evaluated from 200 trajectories with different initial positions.

$$\langle y(t_1)y(t_2)\rangle = \frac{k_BT}{m}[t_1^2E_{2\bar{H},3}(-\gamma t_1^{2\bar{H}}) + t_2^2E_{2\bar{H},3}(-\gamma t_2^{2\bar{H}}) - (t_2-t_1)^2E_{2\bar{H},3}(-\gamma|t_2-t_1|^{2\bar{H}})], \tag{5.1}$$

one can show analytically that, similarly to the FBM, the ensemble-averaged second moment $\langle y^2(t)\rangle$ is identical to its time-averaged analog $\langle\overline{\delta^2(\Delta)}\rangle$ for all Δ in free space, namely,

$$\langle\overline{\delta^2(\Delta,T)}\rangle = 2\frac{k_BT}{m}\Delta^2E_{2\bar{H},3}(-\gamma\Delta^{2\bar{H}}). \tag{5.2}$$

Thus, the time-averaged mean-squared displacement turns over from a ballistic motion

$$\langle\overline{\delta^2(\Delta,T)}\rangle \simeq \Delta^2 \tag{5.3}$$

at short lag time to the subdiffusive behavior

$$\langle\overline{\delta^2(\Delta,T)}\rangle \simeq \Delta^{2-2\bar{H}} \tag{5.4}$$

at long lag times in free space.

We numerically study how this scaling behavior is affected by the confinement. Figure 8 shows typical curves for the time-averaged mean-squared displacement, for interval sizes $L=1/2$, 1, 3, and 100 (regarded as free-space motion) with identical initial conditions and Hurst exponent $\bar{H}=5/8$. The results are summarized as follows. (1) We observe both scaling behaviors, $\langle\overline{\delta^2(\Delta,T)}\rangle \simeq \Delta^2$ turning over to $\simeq\Delta^{2-2\bar{H}}$, for confined FLE motions. (2) For narrow intervals, the curves eventually reach the saturation plateau within the chosen total measurement time T. The saturation values are approximately $L^2/3$. For interval size $L=1/2$, the saturated value is noticeably larger than $L^2/3$, which appears to be caused by multiple reflection events on the walls. The same behavior is observed in the FBM case when considering a large value of $H\geq 1/2$ or very narrow intervals for the given $H=1/4$. (3) As in the case of FBM, the scatter becomes pronounced as the interval length increases.

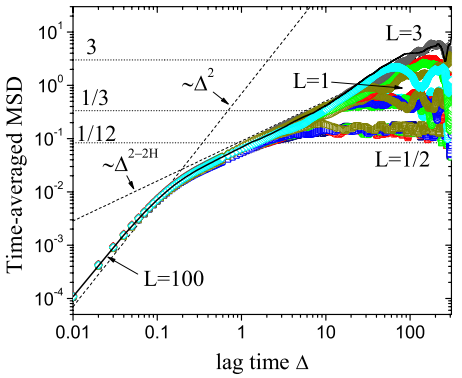

FIG. 8. (Color online) Time-averaged MSD vs lag time Δ. The two dashed lines represent the two asymptotic scaling behaviors $\langle\overline{\delta^2(\Delta,T)}\rangle \simeq \Delta^2$ and $\langle\overline{\delta^2(\Delta,T)}\rangle \simeq \Delta^{2-2\bar{H}}$. For each given $L=1/2$, 1, and 3, five different trajectories are drawn to visualize the scatter. As a reference curve for motion in free space, the curve for $L=100$ (line) is drawn. In the simulation, we chose the Hurst exponent $\bar{H}=5/8$ (NB: for the FLE this means subdiffusion), time increment $dh=0.01$, particle mass $m=1$, initial velocity $v_0=1$, initial position $y_0=0$, friction coefficient $\bar{\gamma}=10$, and $k_BT=1$.

B. Ergodicity-breaking parameter

From a simple argument and simulations, it was shown in Ref. [25]. that the FLE and FBM mean-squared displacements are asymptotically equal, $\langle\overline{\delta^2(y)}\rangle \sim \langle\overline{\delta^2(x^H)}\rangle$, similarly for the ergodicity-breaking parameter, $E_B(y) \sim E_B(x^H)$. Here the asymptotic equivalence is valid at long measurement times T, and the derivation holds for motion in free space. From 200 trajectories of the mean-squared displacement we measure the ergodicity-breaking parameter E_B as function of lag time Δ for interval lengths $L=1/2$, 1, 3, and 100 in Fig. 9. The behavior is similar to the corresponding curves for FBM, displayed in Fig. 3: E_B significantly deviates from the reference curve for free-space motion (i.e., the longer Δ behavior for $L=100$ and the drawn power law $\simeq\Delta$) due to the confinement effect. E_B tends to decrease with smaller L for the same value of Δ. However, the plateau at short lag times that is still observed for $L=100$ (regarded as free-space motion) is due to the initial ballistic motion of FLE. In that

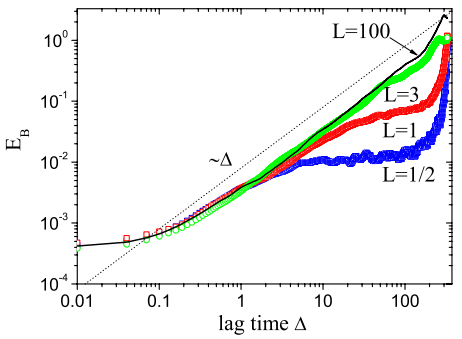

FIG. 9. (Color online) Ergodicity-breaking parameter E_B vs lag time Δ for interval sizes $L=1/2$, 1, 3, and 100. The straight line corresponds to the free-space behavior $E_B \simeq \Delta$. Each curve was obtained from 200 single trajectories, with the same parameter values used in Fig. 8.

regime, the initially directed motion renders the random noise effect negligible.

C. Displacement correlation function

Using the correlation function $\langle y(t_1)y(t_2)\rangle$, we analytically obtain the displacement correlation function in free space in the form (refer to Appendix A for the derivation)

$$\langle \delta y(t,\Delta)\,\delta y(t-\Delta,\Delta)\rangle = 4\frac{k_BT}{m}\Delta^2 E_{2\bar{H},3}[-\gamma(2\Delta)^{2\bar{H}}] - 2\frac{k_BT}{m}\Delta^2 E_{2\bar{H},3}[-\gamma\Delta^{2\bar{H}}], \quad (5.5)$$

so that we observe the following asymptotic behavior:

$$\langle \delta y(t,\Delta)\,\delta y(t-\Delta,\Delta)\rangle \sim \begin{cases} \dfrac{2k_BT}{m\Gamma(3)}\Delta^2, & \text{for } \Delta \to 0 \\ \dfrac{(2^{2-2H}-2)k_BT}{m\gamma\Gamma(3-2\bar{H})}\Delta^{2-2\bar{H}}, & \text{for } \Delta \to \infty, \end{cases} \quad (5.6)$$

where $\delta y(t,\Delta)=y(t+\Delta)-y(t)$. Above expression shows that the displacement correlation has two distinct scaling behaviors. At short lag times, it grows like Δ^2 and is positive due to the ballistic motion. At long lag times, it is negative in the domain $1/2<\bar{H}<1$, exhibiting the same subdiffusive behavior as observed for FBM [cf. Eq. (4.5)] when we replace $H \to 2-2\bar{H}$. Note that to bridge these two scaling behaviors, the displacement correlation passes the zero axis at $\Delta=\Delta_c$ that satisfies $2E_{2\bar{H},3}[-\gamma(2\Delta_c)^{2\bar{H}}]=E_{2\bar{H},3}[-\gamma\Delta_c^{2\bar{H}}]$ in free space. For small γ, we find approximately

$$\Delta_c \approx \left(\frac{\Gamma(2\bar{H}+3)}{2\Gamma(2\bar{H}-1)(2^{2\bar{H}+1}-1)}\frac{m}{\bar{\gamma}}\right)^{1/2\bar{H}}, \quad (5.7)$$

such that it becomes exactly the momentum relaxation time $m/\bar{\gamma}$ for normal Brownian motion ($\bar{H}=1/2$). In the limit $\bar{H} \to 1$, Δ_c goes to infinity to satisfy the equality $2E_{2\bar{H},3}[-\gamma(2\Delta_c)^{2\bar{H}}]=E_{2\bar{H},3}[-\gamma\Delta_c^{2\bar{H}}]$. Thus, Δ_c can be interpreted as the typical time scale for the persistence of the ballistic motion.

Figure 10 shows (a) the displacement correlation versus lag time Δ and (b) the absolute value of the displacement correlation as function of Δ, for $L=1/2$, 1, 3, and 100. The scaling properties derived in Eq. (5.6) are indeed observed. At short lag times, all curves are positive and scale like $\sim\Delta^2$ before decreasing to zero. In the long lag time regime, the displacement correlation becomes negative and the predicted scaling behavior $\simeq\Delta^{2-2\bar{H}}$ is observed. For small intervals ($L=1/2$ and 1), it is saturated due to the confinement effect as seen in the case of FBM.

D. Dimensionality

In the case when the memory tensor is diagonalized, each coordinate motion is independent and FLE motion exhibits

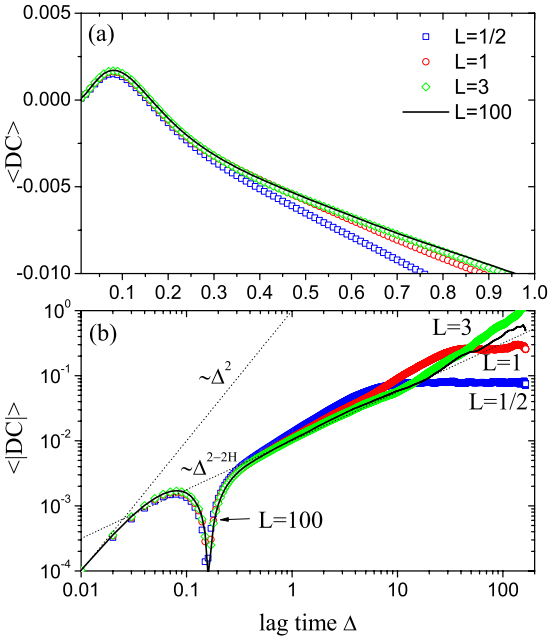

FIG. 10. (Color online) (a) DC vs lag time Δ for $L=1/2$, 1, 3, and 100 (from bottom to top). (b) Absolute value of the displacement correlation as a function of Δ for the given values of L. The two slopes correspond to the limiting behaviors Δ^2 and $\Delta^{2-2\bar{H}}$. In (a) and (b), the ensemble-averaged curves were obtained from 200 different time-averaged displacement correlation curves. Same parameter values as in Fig. 8.

qualitatively the same behavior as shown in the case of FBM with increasing dimensionality. From the mean-squared displacement curves, the same scaling behavior is expected with more elevated amplitude for higher dimensionality. In fact, when each coordinate motion is decoupled, a d-dimensional motion effectively increases the number of single trajectories d times compared to the one-dimensional case. Therefore, the scatter in the mean-square displacement curves decreases with increasing dimensionality and the ergodicity-breaking parameter E_B is expected to follow the relation Eq. (4.7).

VI. CONCLUSION

Motivated by recent single-particle tracking experiments in biological cells, in which confinement due to the rather small cell size becomes relevant, we studied FBM and FLE motions in confined space. In particular, we analyzed the effects of confinement and dimensionality on the stochastic and ergodic properties of the two processes. Interestingly for both stochastic models, the confinement tends to decrease the value of the ergodicity-breaking parameter E_B compared to that in free space. The same trend is observed for increasing dimensionality. Correspondingly, the scatter of time-averaged quantities between individual trajectories is quite small, apart from regimes when the lag time Δ becomes close to the overall measurement time T and the sampling statistics for the corresponding time average become poor. The relaxation of the ergodicity-breaking parameter as function of measurement time is quite similar to previous results in free space. We conclude that neither confinement nor dimensionality effects lead to the appearance of significant ergodicity breaking or scatter between single trajectories.

The displacement correlation function introduced here is a useful quantity that can be easily obtained from single-particle trajectories. It can be used as a tool to discriminate one stochastic model from another. For subdiffusive motion governed by FBM and FLE motion, the displacement correlation should be negative and saturate in the long-measurement time limit due to the confinement. Notably, the negative decrease $(-|\Delta|^{\alpha})$ with lag time Δ and anomalous diffusion exponent α is an intrinsic property of FBM and FLE displacement correlations which is clearly distinguished from that of CTRW subdiffusion. In the latter case, the subdiffusive motion occurs due to the long waiting time distribution between successive jumps and there is no spatial correlation between them so that displacement correlation only fluctuates around zero with time. FLE motion can be distinguished from FBM motion since the displacement correlation has a positive value at short times due to the ballistic motion in the FLE model.

ACKNOWLEDGMENTS

We thank Stas Burov and Eli Barkai for helpful and enjoyable discussions. Financial support from the DFG is acknowledged.

APPENDIX A: DERIVATION OF THE DISPLACEMENT CORRELATION FUNCTION

In this appendix, we derive analytical expressions for the displacement correlations, Eqs. (4.5) and (5.5). For a stochastic variable x, we define

$$\delta x(t,\Delta) = x(t+\Delta) - x(t). \tag{A1}$$

The displacement correlation is then given by

$$\langle \delta x(t,\Delta)\,\delta x(t-\Delta,\Delta)\rangle = \langle x(t+2\Delta)x(t+\Delta)\rangle - \langle x(t+2\Delta)x(t)\rangle - \langle x(t+\Delta)^2\rangle + \langle x(t+\Delta)x(t)\rangle. \tag{A2}$$

We now calculate this expression for FBM and FLE motions.

1. FBM

For FBM $[x(t)=x^H(t)]$, we use the expression

$$\langle x(t_1)x(t_2)\rangle = K_H(t_1^{2H} + t_2^{2H} - |t_2 - t_1|^{2H}) \tag{A3}$$

for the autocorrelation. With this, we readily obtain the result

$$\langle \delta x(t,\Delta)\,\delta x(t-\Delta,\Delta)\rangle = K_H(2^{2H} - 2)\Delta^{2H}. \tag{A4}$$

2. FLE

For FLE $[x(t)=y(t)]$, we use the correlation function [55]

$$\langle x(t_1)x(t_2)\rangle = \frac{k_B T}{m}[t_1^2 E_{2\bar{H},3}(-\gamma t_1^{2\bar{H}}) + t_2^2 E_{2\bar{H},3}(-\gamma t_2^{2\bar{H}}) - (t_2 - t_1)^2 E_{2\bar{H},3}(-\gamma|t_2 - t_1|^{2\bar{H}})]. \tag{A5}$$

The displacement correlation is then obtained as

$$\langle \delta x(t,\Delta)\,\delta x(t-\Delta,\Delta)\rangle = \frac{4k_BT}{m}\Delta^2 E_{2\bar{H},3}[-\gamma(2\Delta)^{2\bar{H}}] - \frac{2k_BT}{m}\Delta^2 E_{2\bar{H},3}[-\gamma\Delta^{2\bar{H}}]. \quad \text{(A6)}$$

Expanding the generalized Mittag-Leffler function $E_{2\bar{H},3}(x) \approx 1/\Gamma(3)+x/\Gamma(2\bar{H}+3)+\cdots$ for $x \ll 1$, the displacement correlation is approximated as

$$\langle \delta x(t,\Delta)\,\delta x(t-\Delta,\Delta)\rangle \sim \frac{2}{\Gamma(3)}\frac{k_BT}{m}\Delta^2 \quad \text{(A7)}$$

at short lag times. With the expansion $E_{2\bar{H},3}(-x) \approx 1/x\Gamma(3-2\bar{H})$ for $x \gg 1$, the long lag time behavior of the displacement correlation is obtained as

$$\langle \delta x(t,\Delta)\,\delta x(t-\Delta,\Delta)\rangle \sim \frac{2^{2-2\bar{H}}-2}{\gamma\Gamma(3-2\bar{H})}\frac{k_BT}{m}\Delta^{2-2\bar{H}}. \quad \text{(A8)}$$

Note that the prefactor $(2^{2-2\bar{H}}-2)/\Gamma(3-2\bar{H})$ is zero for $\bar{H}=1/2$ and then becomes increasingly negative, saturating at the value -1 for $\bar{H}=1$.

APPENDIX B: DERIVATION OF Eq. (4.7)

From the definition of the time-averaged mean-squared displacement, Eq. (4.6), we expand $\langle[\overline{\delta^2(\Delta,T)}]^2\rangle$ in the form

$$\langle[\overline{\delta^2(\Delta,T)}]^2\rangle = \frac{1}{(T-\Delta)^2}\int_0^{T-\Delta}\int_0^{T-\Delta}\left\{\sum_{i=1}^{d}\langle[x_i^H(t_1+\Delta)-x_i^H(t_1)]^2[x_i^H(t_2+\Delta)-x_i^H(t_2)]^2\rangle + \sum_{i\neq j}\langle[x_i^H(t_1+\Delta)-x_i^H(t_1)]^2\rangle\langle[x_j^H(t_2+\Delta)-x_j^H(t_2)]^2\rangle\right\}dt_1dt_2. \quad \text{(B1)}$$

Using the Isserlis theorem for Gaussian process with zero mean [48]

$$\langle x(t_1)x(t_2)x(t_3)x(t_4)\rangle = \langle x(t_1)x(t_2)\rangle\langle x(t_3)x(t_4)\rangle + \langle x(t_1)x(t_3)\rangle\langle x(t_2)x(t_4)\rangle + \langle x(t_1)x(t_4)\rangle\langle x(t_2)x(t_3)\rangle, \quad \text{(B2)}$$

the first term in the braces in Eq. (B1) can be rewritten as

$$\sum_{i=1}^{d}\langle[x_i^H(t_1+\Delta)-x_i^H(t_1)]^2[x_i^H(t_2+\Delta)-x_i^H(t_2)]^2\rangle = \sum_{i=1}^{d}\langle[x_i^H(t_1+\Delta)-x_i^H(t_1)]^2\rangle\langle[x_i^H(t_2+\Delta)-x_i^H(t_2)]^2\rangle + 2\sum_{i=1}^{d}\langle[x_i^H(t_1+\Delta)-x_i^H(t_1)][x_i^H(t_2+\Delta)-x_i^H(t_2)]\rangle^2. \quad \text{(B3)}$$

In this expression, we note that the sum of the second term in Eq. (B1) and the first term in Eq. (B3) yields $\langle\overline{\delta^2(\Delta,T)}\rangle^2$,

$$\langle\overline{\delta^2(\Delta,T)}\rangle^2 = \frac{d^2}{(T-\Delta)^2}\int_0^{T-\Delta}\int_0^{T-\Delta}\langle[x^H(t_1+\Delta)-x^H(t_1)]^2\rangle\times\langle[x^H(t_2+\Delta)-x^H(t_2)]^2\rangle dt_1dt_2 = d^2\langle\overline{\delta^2}\rangle_{1D}^2, \quad \text{(B4)}$$

where we used the property

$$\sum_{i,j}\langle[x_i^H(t_1+\Delta)-x_i^H(t_1)]^2\rangle\langle[x_j^H(t_2+\Delta)-x_j^H(t_2)]^2\rangle = d^2\langle[x^H(t_1+\Delta)-x^H(t_1)]^2\rangle\langle[x^H(t_2+\Delta)-x^H(t_2)]^2\rangle \quad \text{(B5)}$$

due to the independence of the motion in each coordinate direction. We also note that the expression $\langle[\overline{\delta^2(\Delta,T)}]^2\rangle - \langle\overline{\delta^2(\Delta,T)}\rangle^2$ simplifies to

$$\langle[\overline{\delta^2(\Delta,T)}]^2\rangle - \langle\overline{\delta^2}\rangle^2 = \frac{2}{(T-\Delta)^2}\sum_{i=1}^{d}\int_0^{T-\Delta}\int_0^{T-\Delta}\langle[x_i^H(t_1+\Delta)-x_i^H(t_1)][x_i^H(t_2+\Delta)-x_i^H(t_2)]\rangle^2 dt_1dt_2 = d[\langle(\overline{\delta^2})^2\rangle_{1D} - \langle\overline{\delta^2}\rangle_{1D}^2]. \quad \text{(B6)}$$

From Eqs. (B4) and (B6), the ergodicity-breaking parameter follows the general relation

$$E_B(d) = \frac{\langle[\overline{\delta^2(\Delta,T)}]^2\rangle - \langle\overline{\delta^2(\Delta,T)}\rangle^2}{\langle\overline{\delta^2(\Delta,T)}\rangle^2} = \frac{E_B(d=1)}{d}. \quad \text{(B7)}$$

[1] R. Metzler and J. Klafter, Phys. Rep. **339**, 1 (2000); J. Phys. A **37**, R161 (2004).

[2] H. Scher and E. W. Montroll, Phys. Rev. B **12**, 2455 (1975).

[3] J. W. Kirchner, X. Feng, and C. Neal, Nature (London) **403**, 524 (2000); H. Scher, G. Margolin, R. Metzler, J. Klafter, and B. Berkowitz, Geophys. Res. Lett. **29**, 1061 (2002).

[4] F. Mainardi, M. Raberto, R. Gorenflo, and E. Scalas, Physica A **287**, 468 (2000).

[5] I. Y. Wong, M. L. Gardel, D. R. Reichman, E. R. Weeks, M. T. Valentine, A. R. Bausch, and D. A. Weitz, Phys. Rev. Lett. **92**, 178101 (2004).

[6] E. Fischer, R. Kimmich, and N. Fatkullin, J. Chem. Phys. **104**, 9174 (1996).

[7] E. R. Weeks, J. C. Crocker, A. C. Levitt, A. Schofield, and D. A. Weitz, Science **287**, 627 (2000).

[8] I. Golding and E. C. Cox, Phys. Rev. Lett. **96**, 098102 (2006).

[9] I. M. Tolić-Nørrelykke, E. L. Munteanu, G. Thon, L. Oddershede, and K. Berg-Sørensen, Phys. Rev. Lett. **93**, 078102 (2004).
[10] A. Caspi, R. Granek, and M. Elbaum, Phys. Rev. Lett. **85**, 5655 (2000); Phys. Rev. E **66**, 011916 (2002).
[11] G. Seisenberger, M. U. Ried, T. Endreß, H. Büning, M. Hallek, and C. Bräuchle, Science **294**, 1929 (2001).
[12] I. Bronstein, Y. Israel, E. Kepten, S. Mai, Y. Shav-Tal, E. Barkai, and Y. Garini, Phys. Rev. Lett. **103**, 018102 (2009).
[13] M. Weiss, M. Elsner, F. Kartberg, and T. Nilsson, Biophys. J. **87**, 3518 (2004); M. Weiss, H. Hashimoto, and T. Nilsson, *ibid.* **84**, 4043 (2003). HeLa cells belong to an immortal cell line derived from cancer cells originally taken from patient Henrietta Lacks in 1951.
[14] V. Tejedor and R. Metzler, J. Phys. A (to be published).
[15] S. Havlin and D. ben-Avraham, Adv. Phys. **36**, 695 (1987).
[16] A. Klemm, R. Metzler, and R. Kimmich, Phys. Rev. E **65**, 021112 (2002).
[17] G. M. Molchan, Commun. Math. Phys. **205**, 97 (1999).
[18] I. Goychuk and P. Hänggi, Phys. Rev. Lett. **99**, 200601 (2007).
[19] S. Chaudhury and B. J. Cherayil, J. Chem. Phys. **125**, 024904 (2006); S. Chaudhury, D. Chatterjee, and B. J. Cherayil, *ibid.* **129**, 075104 (2008).
[20] O. Yu. Slyusarenko, V. Yu. Gonchar, A. V. Chechkin, I. M. Sokolov, and R. Metzler (unpublished).
[21] I. Goychuk, Phys. Rev. E **80**, 046125 (2009).
[22] S. Burov and E. Barkai, Phys. Rev. Lett. **100**, 070601 (2008).
[23] Y. He, S. Burov, R. Metzler, and E. Barkai, Phys. Rev. Lett. **101**, 058101 (2008); A. Lubelski, I. M. Sokolov, and J. Klafter, *ibid.* **100**, 250602 (2008).
[24] R. Metzler, V. Tejedor, J.-H. Jeon, Y. He, W. Deng, S. Burov, and E. Barkai, Acta Phys. Pol. B **40**, 1315 (2009).
[25] W. Deng and E. Barkai, Phys. Rev. E **79**, 011112 (2009).
[26] J.-D. Bao, P. Hänggi, and Y.-Z. Zhuo, Phys. Rev. E **72**, 061107 (2005).
[27] S. Burov, R. Metzler, and E. Barkai (unpublished).
[28] T. Neusius, I. M. Sokolov, and J. C. Smith, Phys. Rev. E **80**, 011109 (2009).
[29] A. N. Kolmogorov, Dokl. Akad. Nauk SSSR **26**, 115 (1940).
[30] A. M. Yaglom, Am. Math. Soc. Transl. **8**, 87 (1958).
[31] B. B. Mandelbrot, Compt. Rend. **260**, 3274 (1965).
[32] B. B. Mandelbrot and J. W. van Ness, SIAM Rev. **10**, 422 (1968).
[33] H. E. Hurst, Trans. Am. Soc. Civ. Eng. **116**, 770 (1951); H. E. Hurst, R. O. Black, and Y. M. Simaika, *Long Term Storage: An Experimental Study* (Constable, London, 1965).
[34] I. Adelman, Am. Econ. Rev. **60**, 444 (1965); C. W. J. Granger, Econometrica **34**, 150 (1966).
[35] J. Szymanski and M. Weiss, Phys. Rev. Lett. **103**, 038102 (2009).
[36] V. Tejedor, O. Bénichou, R. Voituriez, R. Jungmann, F. Simmel, C. Selhuber, L. Oddershede, and R. Metzler, Biophys. J. (to be published).
[37] F. Biagini, Y. Hu, B. Øksendal, and T. Zhang, *Stochastic Calculus for Fractional Brownian Motion and Applications* (Springer, Berlin, 2008).
[38] A. Weron and M. Magdziarz, Europhys. Lett. **86**, 60010 (2009).
[39] H. Qian, in *Process with Long-Range Correlations: Theory and Applications*, edited by G. Rangarajan and M. Z. Ding, Lecture Notes in Physics Vol. 621 (Springer, New York, 2003).
[40] S. C. Kou and X. S. Xie, Phys. Rev. Lett. **93**, 180603 (2004).
[41] The autocorrelation function for $0<H<1/2$ becomes positive at $t_1=t_2$ due to the second term in Eq. (2.6) and has the property $\int_{-\infty}^{\infty}dt\langle\xi^H(t)\xi^H(0)\rangle=0$.
[42] J. Feder, *Fractals* (Plenum Press, New York, 1988); B. B. Mandelbrot, *The Fractal Geometry of Nature* (W. H. Freeman and Company, New York, 1977).
[43] J. Unterberger, Ann. Probab. **37**, 565 (2009).
[44] H. Qian, G. M. Raymond, and J. B. Bassingthwaighte, J. Phys. A **31**, L527 (1998).
[45] K. Falconer, *Fractal Geometry: Mathematical Foundations and Applications* (Wiley, Chichester, UK, 1990).
[46] P. Langevin, Compt. Rend. **146**, 530 (1908).
[47] N. G. van Kampen, *Stochastic Processes in Physics and Chemistry* (North-Holland, Amsterdam, 1981).
[48] W. T. Coffey, Y. P. Kalmykov, and J. T. Waldron, *The Langevin Equation: With Applications to Stochastic Problems in Physics, Chemistry and Electrical Engineering*, 2nd ed. (World Scientific, Singapore, 2003).
[49] R. Zwanzig, *Nonequilibrium Statistical Mechanics* (Oxford University Press, Oxford, UK, 2001).
[50] R. Kubo, in *Tokyo Lectures in Theoretical Physics*, edited by R. Kubo (W. A. Benjamin, Inc., New York, 1966).
[51] B. J. Berne, J. P. Boon, and S. A. Rice, J. Chem. Phys. **45**, 1086 (1966).
[52] I. Podlubny, *Fractional Differential Equations* (Academic Press, New York, 1998).
[53] *Bateman Manuscript Project: Higher Transcendental Functions*, edited by A. Erdélyi (McGraw-Hill Book Co., New York, 1955), Vol. III.
[54] E. Lutz, Phys. Rev. E **64**, 051106 (2001).
[55] N. Pottier, Physica A **317**, 371 (2003).
[56] J. R. M. Hosking, Water Resour. Res. **20**, 1898 (1984).
[57] K. Diethelm, N. J. Ford, and A. D. Freed, Nonlinear Dyn. **29**, 3 (2002).